

Numerical study of three-dimensional turbulent natural convection in a differentially heated air-filled tall cavity[☆]

Hongxing Yang^{a,*}, Zuojin Zhu^b

^a Department of Building Services Engineering, The Hong Kong Polytechnic University, Hong Kong, China

^b The State Key Lab of Fire Science, Department of Thermal Science and Energy Engineering, USTC, Hefei, 230026, China

Available online 29 February 2008

Abstract

Correct description of turbulent natural convection plays an important role in the field of heat transfer and building environment. The natural convection in turbulent regime in a tall cavity can exhibit a complex dynamic behavior that affects the momentum and heat transport between the hot and cold vortical clusters. Using higher order finite difference numerical scheme, the results from this numerical study present the vortical structures in the tall cavity when the height–depth–width ratio is 16:8:1 for higher Rayleigh numbers and the characteristics of the correlation between the velocity components along the horizontal and vertical center lines in the midplane.

© 2008 Published by Elsevier Ltd.

Keywords: Turbulent natural convection; Air-filled tall cavity; Vortical clusters

1. Introduction

Natural convection is a heat transfer of buoyancy induced flow. Because turbulence is still a complex physical problem not well resolved due to the chaotically flow structure having a broad range of space and time scales [1], the natural convection in a turbulent regime requires more research efforts. Even though turbulence modeling [2] has a long history, so far it is still difficult to address a significant progress well satisfied by both the theoretical and applied researchers. To get a grip on turbulence, the lattice Boltzmann equation (LBZ)[3] is useful to introduce a new approach that facilitates numerical simulation of complex flows at high Reynolds numbers. However, this method requires time to carefully validate and the particular experience to utilize.

Facing to the recent development of turbulence study and considering the hydrodynamic turbulence should satisfy the Navier–Stokes equations, we incline to present a coarse grid

direct numerical simulation (DNS) to study the three-dimensional turbulent natural convection in the tall cavity in a personal computer by holding the Boussinesq approximation. As reported in our previous work [4], the traditionally means DNS should use a very fine grid in general causing the computational demands exceed the capability of a personal computer. Fortunately, a novel idea based on the nonstandard analysis for the description of turbulence has been recently proposed [5,6]. This implies that the numerical results with respect to coarse grid DNS may be promising [4,7].

A brief literature review of the natural convection in a tall cavity has been given in our previous numerical work [8], where, the laminar natural convection regime was highlighted. In addition, recent experiments have investigated the natural convection in a tall cavity in turbulent [9] and transitional regimes [10]. The former has presented the temperature and velocity profiles as well as the heat fluxes and Reynolds stresses for the cases of Rayleigh numbers equal to 0.86×10^6 and 1.43×10^6 , while the latter has shown the transitional patterns obtained by using the interferometry at the Rayleigh number ranging from 10^4 to 5×10^4 .

In this paper, we focus on the numerical investigation of the turbulent natural convection of air in a tall cavity at the Rayleigh number ranging from 2×10^5 to 4×10^6 . The objective is to

[☆] Communicated by W.J. Minkowycz.

* Corresponding author.

E-mail address: behxyang@polyu.edu.hk (H. Yang).

Nomenclature

A	H/W , the height to width ratio
D	Depth of the tall cavity, m
g	Gravitational acceleration, m^2/s
H	Height of the cavity, m
Nu_{av}	Face-time-averaged Nusselt number
p	Pressure
Pr	Prandtl number of fluid
Ra	Rayleigh number
t	Time
T_h	Absolute temperature of the hot vertical wall K
T_c	Absolute temperature of the cold vertical wall K
\mathbf{u}	Velocity vector
U	Velocity component in x -direction
V	Velocity component in y -direction
W	Velocity component in z -direction
W	Width of the cavity m

Greek symbols

β_T	Coefficient of volumetric expansion
ΔT	$T_h - T_c$, Temperature difference between the two vertical walls
κ	Thermal diffusivity, m^2/s
ρ	Mean density of the fluid, kg/m^3
Θ	Normalized temperature
ν	Kinematic viscosity, m^2/s

Subscripts

c	cold
h	hot
l	left vertical wall
r	right vertical wall

examine the heat and fluid flow characteristics in the differentially heated air-filled tall cavity when the thermal induced flow becomes fully turbulent.

2. Governing equations and numerical method

Consider the natural convection problem as schematically shown in Fig. 1, following the procedure given in Refs. [4,8], the governing equations in a three-dimensional Cartesian coordinate system (x,y,z) are as follows:

$$\nabla \cdot \mathbf{u} = 0 \tag{1}$$

$$\mathbf{u}_t + (\mathbf{u} \cdot \nabla)\mathbf{u} = -\nabla p + \Theta \boldsymbol{\lambda} + (Ra Pr)^{-1/2} \nabla^2 \mathbf{u} \tag{2}$$

$$\Theta_t + (\mathbf{u} \cdot \nabla)\Theta = (Ra/Pr)^{-1/2} \nabla^2 \Theta \tag{3}$$

where $\boldsymbol{\lambda} = (0, 1, 0)$ denotes the unit vector in the vertical direction, and Pr is the Prandtl number, with the Rayleigh number $Ra = g\beta_T$

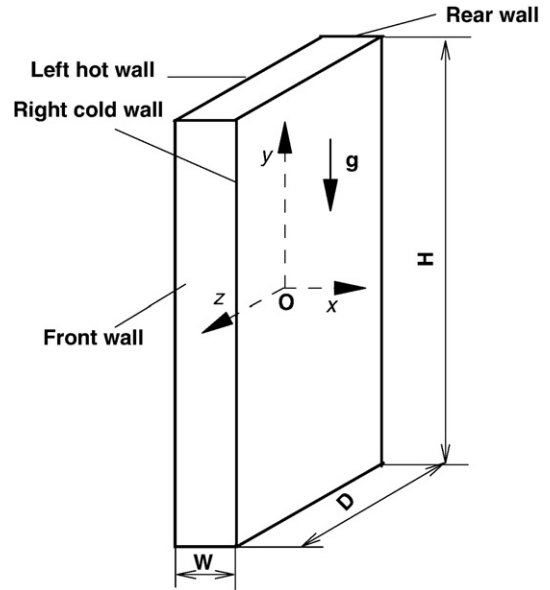


Fig. 1. Schematic diagram of the differentially heated tall cavity.

$(T_h - T_c)H^3 / (\nu\kappa)$. The solutions of the governing Eqs. (1–3) are sought with appropriate conditions that are compatible with the considered problem. As aforementioned, the boundary conditions on the two vertical walls can be written as

$$U = 0, V = 0, W = 0, \Theta = 0.5, \text{ for } x = -0.5, y \in (-8, 8), z \in (-4, 4) \tag{4}$$

and

$$U = 0, V = 0, W = 0, \Theta = -0.5, \text{ for } x = 0.5, y \in (-8, 8), z \in (-4, 4). \tag{5}$$

For the horizontal walls, we have

$$U = 0, V = 0, W = 0, \partial\Theta/\partial y = 0, \text{ for } y = \pm 8, x \in (-0.5, 0.5), z \in (-4, 4) \tag{6}$$

with

$$U = 0, V = 0, W = 0, \partial\Theta/\partial z = 0, \text{ for } z = \pm 4, x \in (-0.5, 0.5), y \in (-8, 8) \tag{7}$$

for the boundary conditions on the front and rear vertical walls. The initial condition in the tall cavity is given by

$$U = 0, V = 0, W = 0, \Theta = 0. \tag{8}$$

The method to solve the 3D unsteady Boussinesq-type Navier–Stokes equations is the accurate projection method (PmIII) developed by Brown et al. [11]. A non-uniform staggered grid system is used in the numerical simulation. The solution method has been used to study the turbulent Rayleigh–Benard convection [4], where the method for the discretization of the convective terms in the governing equations was omitted.

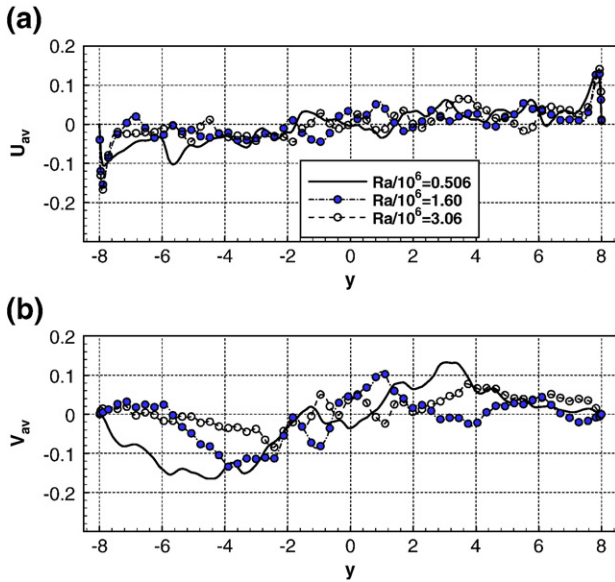


Fig. 2. Time-averaged velocity distributions along the vertical centerline in the midplane of $z=0$ for three Rayleigh numbers ((a) U_{av} ; (b) V_{av}).

For the finite difference scheme, the process of discretization of the term UU_x in Eq. (2) is taken as a special example here. Assuming that the velocity component (U_{ijk}) is located at $(x_{i-1/2}, y_j, z_k)$, $\alpha_i (i=1,4)$ are the finite difference coefficients that can be derived from the Taylor expansion, and for positive velocity component $U_{ijk} > 0$, the fourth order upwind scheme can be expressed as

$$(UU_x)_{ijk} = U_{ijk} [-(\alpha_1 + \alpha_2 + \alpha_3)U_{ijk} + \alpha_1 U_{i-1,j,k} + \alpha_2 U_{i-2,j,k} + \alpha_3 U_{i+1,j,k}] - \alpha_4 U_{ijk} (U_{xxx})_{ijk}. \quad (9)$$

If $h_i = x_{i-1/2} - x_{i-1/2-1}$, according to the Taylor expansion of the velocities at point $(i-1, j, k)$, $(i-2, j, k)$ and $(i+1, j, k)$, the following coefficients of the scheme can be found

$$\alpha_2 = \frac{s_3^3 + s_2^3}{h_i \Delta}, \quad \alpha_3 = -\frac{s_2^3 - s_3^3}{h_i \Delta}, \quad \alpha_1 = -\alpha_2 s_2^2 - \alpha_3 s_3^2 \quad (10)$$

$$\alpha_4 = \left(\alpha_1 h_i^4 + \alpha_2 (h_i + h_{i-1})^4 + \alpha_3 h_{i+1}^4 \right) / 24 \quad (11)$$

where $s_2 = (h_{i-1} + h_i) / h_i$, $s_3 = h_{i+1} / h_i$, and $\Delta = s_2 s_3 (s_2 - 1) (s_3 + 1) (s_3 + s_2)$. Similar expressions can be derived for the upwind differencing of other convective terms in the energy and momentum of Eqs. (2), (3). It is noted that the fourth order derivative of \mathbf{u} can be discretized by the central difference approach, which is used for treating the diffusion terms in the governing equations. Referring to the overall solution procedure [12], the main difference is in the discretization process of the convective terms.

3. Results and discussion

The numerical solutions of the turbulent natural convection in a differentially heated air-filled tall cavity with the height–

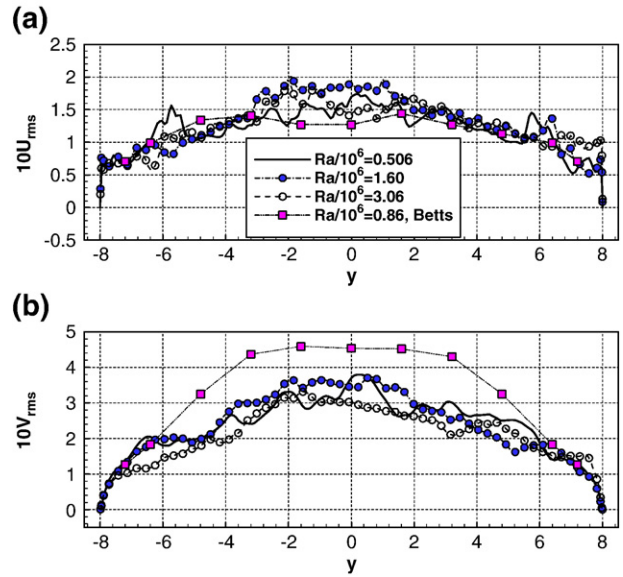


Fig. 3. Distributions of root mean square values of velocity components along the vertical centerline in the midplane of $z=0$ at three Rayleigh numbers ((a) $10U_{rms}$; (b) $10V_{rms}$).

depth–width ratio 16:8:1 were obtained by virtue of coarse grid DNS. Each scenario was investigated in two temporal stages. Each stage contains 20,000 time-steps with a time-step of 0.004. The terminated computational time is $t=160$.

The results are discussed in terms of four particular aspects: velocities, temperatures, and flow fields and heat transfer. The natural convection in the tall cavity at the Ra ranging from 2×10^5 to 4×10^6 is really in turbulent regime. The face-time-average Nusselt numbers on the heating and cooling walls follow a power law with an index of 0.25, and the correlation

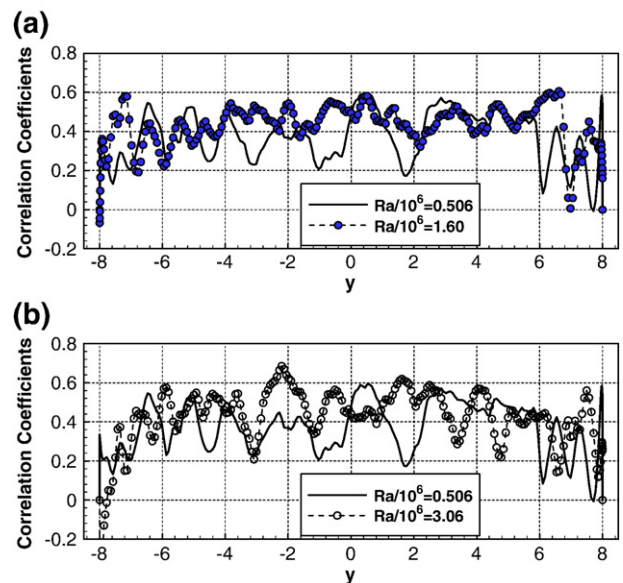


Fig. 4. Distributions of correlation coefficients of velocity components U and V along the vertical centerline in the midplane of $z=0$ for three Rayleigh numbers ((a) $Ra/10^6 = 0.506, 1.60$; (b) $Ra/10^6 = 0.506, 3.06$).

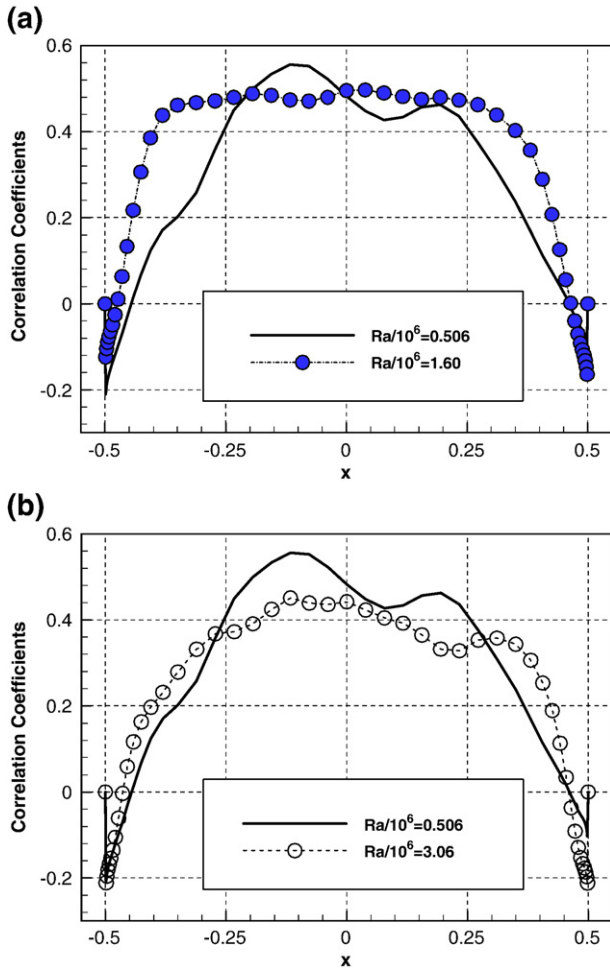


Fig. 5. Distributions of correlation coefficients of velocity components U and V along the horizontal centerline in the midplane of $z=0$ for three Rayleigh numbers ((a) $Ra/10^6=0.506, 3.06$; (b) $Ra/10^6=0.506, 16$).

coefficients of horizontal and vertical velocity components in the two centerlines of the midplane ($z=0$) have distributions depending on the Rayleigh number, and fluctuate around 0.4.

3.1. Velocity

Over the time range from $t=30$ to $t=160$, the time-averaged large velocities (Fig. 2(a)–(b)) and their root mean square values (Fig. 3(a)–(b)) in the vertical centerline of the spanwise midplane ($z=0$) were obtained. The time-averaged velocity curves in the vertical centerline (Fig. 2(a)–(b)) behave in a spatial wavy oscillation due to stretching and folding of the large spanwise vortices. As illustrated in Fig. 2(a), due to the constrain of the top and bottom walls, the averaged velocity U_{av} has two peaks, showing the presence of the wall jet flow turns. The spatial wave number and the velocity peak values for the U_{av} curve in the vertical centerline are closely dependent on the Rayleigh number. It can be seen from Fig. 2(b), the dependence of the time-averaged velocity V_{av} in the vertical centerline on Ra is more evident than that of the horizontal velocity component U_{av} in the vertical centerline.

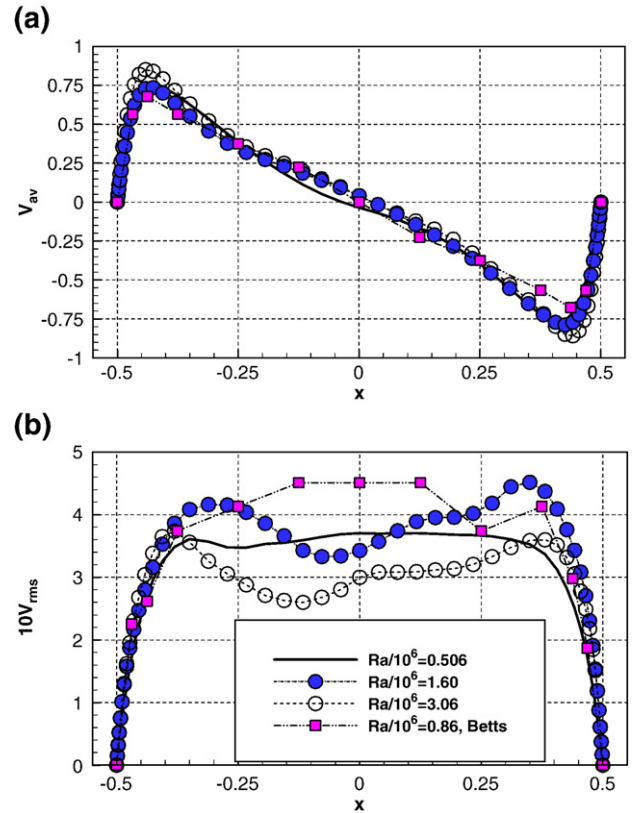


Fig. 6. Distributions of time-averaged velocity component and their rms values along the horizontal centerline in the midplane of $z=0$ for three Rayleigh numbers ((a) V_{av} ; (b) $10V_{rms}$).

Fig. 3(a)–(b) shows that in the vertical centerline the root mean square (rms) curves of the two velocity components are also characterized by spatial oscillation, and the Ra dependence. Comparison with recent measurement [9] indicates that the rms

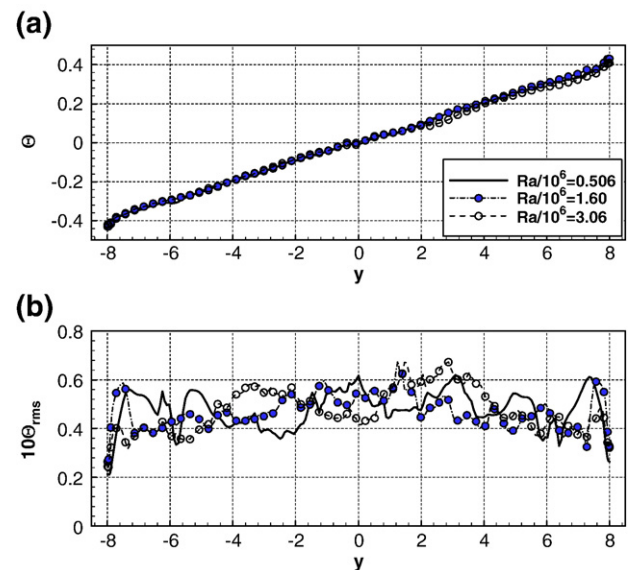


Fig. 7. Distributions of the time-averaged temperature and the relevant root mean square value along the vertical centerline in the midplane of $z=0$ for three Rayleigh numbers ((a) Θ_{rms} ; (b) $10\Theta_{rms}$).

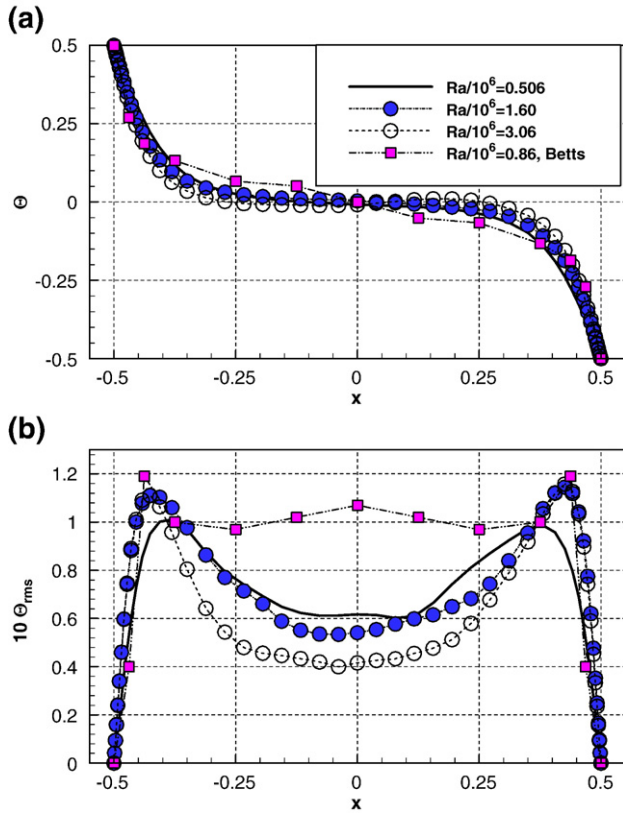


Fig. 8. Distributions of the time-averaged temperature and the relevant root mean square value along the horizontal centerline in the midplane of $z=0$ for three Rayleigh numbers (a) Θ_{rms} ; (b) $10\Theta_{rms}$).

values of velocity U and V in the centerline are consistent with the measured data quite well.

The velocity components in the vertical and horizontal directions in the vertical and horizontal centerlines in the spanwise midplane ($z=0$) are mutually coupled with a correlation coefficient oscillating around a value of 0.4, as shown in Figs. 4 and 5. This particular velocity correlating phenomenon is coincident with the suggestions from Tennekes and Lumley [15] that the correlation coefficient has a value of approximately 0.4 in a fully turbulent flow. However, the present numerical results show that this note is merely correct in the means of average. Actually, for the turbulent natural convection in the tall cavity, the correlation coefficient of different velocity components depends on the flow structures.

The spatial fluctuation of the velocity correlation coefficient in the vertical centerline conceals the flow characteristics of the turbulent natural convection in a tall cavity. While the negative velocity correlation near the top and bottom walls implies the inverse cascade of turbulent kinetic energy from small scale to large scale eddies. From Fig. 5, it is seen that the distribution of the velocity correlation coefficient in the horizontal centerline of the midplane depends on the Rayleigh number.

Because the height to width aspect ratio is rather large ($H/W=16$), the two vertical wall jets have an evidently strong

interaction, resulting in multi-cellular vortical structures in the central region of the tall cavity. These cellular structures lead to spatial fluctuation of the time-averaged velocity components, i.e. the wavy rms curves and the spatial oscillation of the correlation coefficient of the two velocity components in the vertical centerline of the midplane ($z=0$).

On the other hand, as given in Fig. 6(a), the time-averaged vertical velocity component curve in the horizontal centerline of the midplane ($z=0$) fits well with the measured curve from Betts and Bokhari [9]. The peaks near the vertical walls obtained by numerical method are slightly higher than those of the measured data. The time-averaged velocity V_{av} curves are almost insensitive to the Rayleigh number. However, as shown in Fig. 6(b), despite the good fitting of the rms values of V from the calculation near the walls with the measured data, there is a large deviation in the central region of the horizontal centerline. Furthermore, in contrast to V_{rms} distribution in the near wall region, the V_{rms} curve in the central region of the horizontal centerline is quite sensitive to the Rayleigh number.

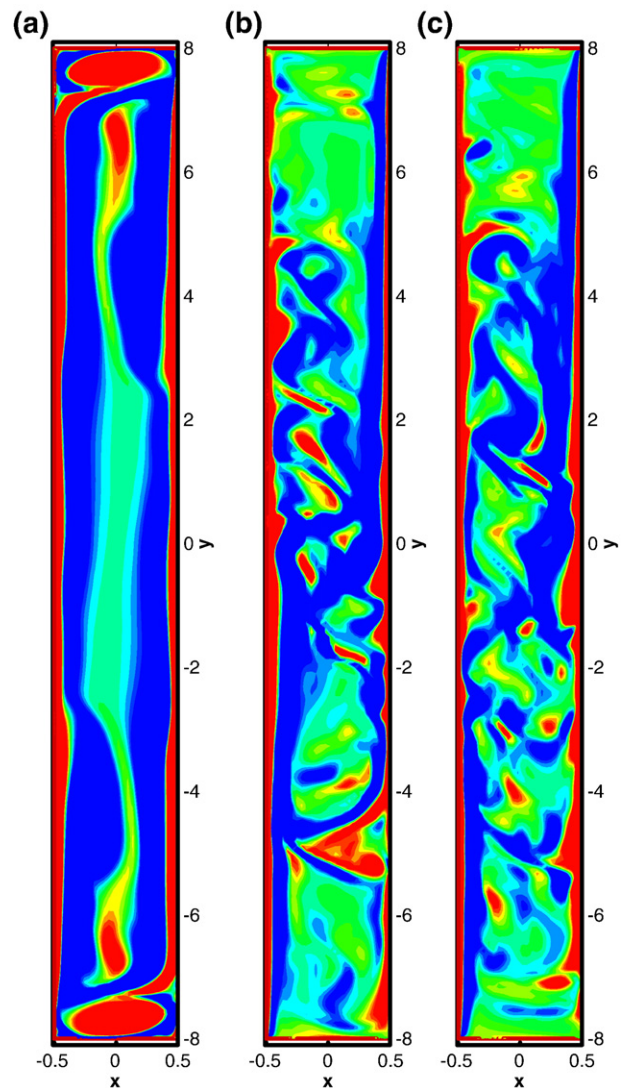


Fig. 9. Flow patterns of vorticity field ω_z in the midplane of $z=0$ for $Ra=1.60 \times 10^6$ ((a) $t=20$, (b) $t=100$, (c) $t=160$).

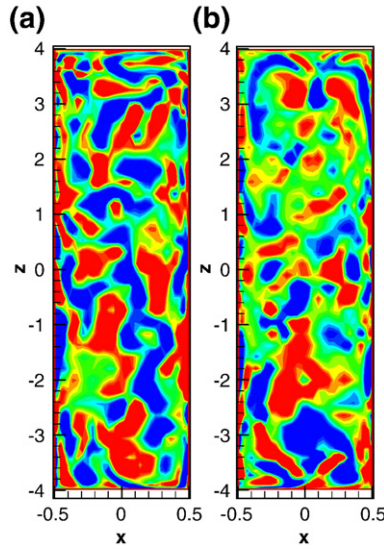


Fig. 10. Flow patterns of vorticity field ω_y in the midplane of $y=0$ for $Ra=1.60 \times 10^6$ ((a) $t=80$, (b) $t=160$).

3.2. Temperature

The time-averaged temperature in the vertical centerline of the midplane ($z=0$) distributes almost linearly when the top and bottom walls are kept adiabatic as shown in Fig. 7(a). Furthermore, the effect of Rayleigh number on this averaged temperature distribution is negligible. However, as indicated in Fig. 7(b), significant influence of Ra on the rms of temperature can be observed. The spatially wavy rms curve of temperature indicates the appearance of the cellular flow structures in the cavity.

The temperature's rms in the vertical centerline fluctuate around 0.05, but the temperature's rms on the top and bottom walls are relatively low. Similarly, as shown in Fig. 8(a), the Ra 's effect on the time-averaged temperature is much smaller than that on the relevant temperature rms curve in the horizontal centerline of the mod plane ($z=0$). The averaged temperature profile in the centerline coincides well with the

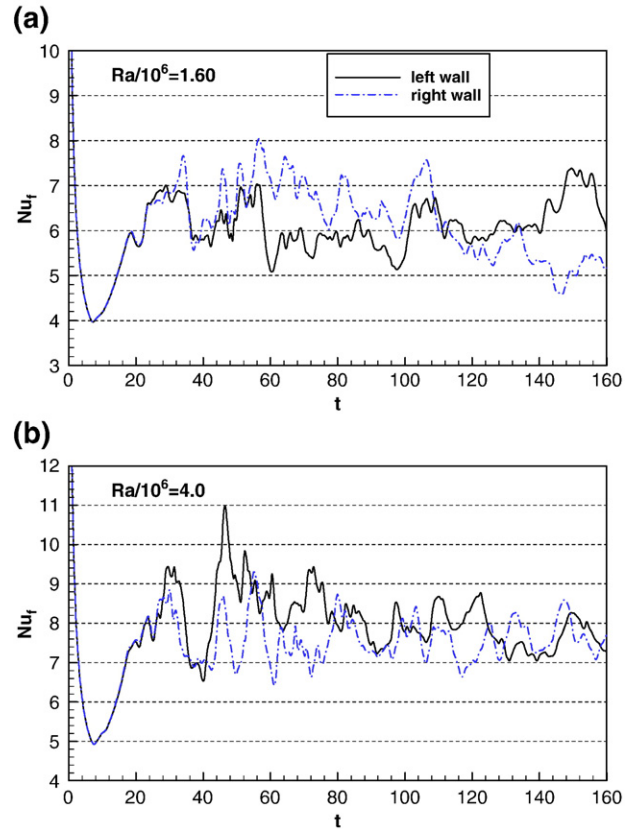


Fig. 11. Evolutions of face Nusselt numbers when (a) $Ra=1.6 \times 10^6$ and (b) $Ra=4.0 \times 10^6$.

measured profile [9]. However, there is a large difference for the comparison between the calculated and measured temperature rms curves in the central region of the horizontal centerline as shown in Fig. 8(b), which indicates that the simulated hot and cold vortical clusters in the region have no more extensive interaction than that in the experiment of Betts and Bokhari [9]. The rms of temperature in the central region depends on the Rayleigh number and the calculated rms of temperature at the origin in Fig. 8(b) is identical to that in Fig. 7(b).

Table 1
Dependence of face-time-averaged Nusselt number on the Rayleigh number for $H/W=16$

Numerical results					Experimental results	
$Ra/10^5$	$Nu_{av,l}$	$Nu_{av,r}$	$rms(Nu_{av,l})$	$rms(Nu_{av,r})$	Nu_{exp}^a	Nu_{exp}^b
2.00	3.66	3.57	0.251	0.249	3.807	3.771
3.55	4.07	4.30	0.377	0.307	4.394	4.51
5.06	4.69	4.57	0.280	0.348	4.801	5.038
9.07	5.21	5.52	0.398	0.456	5.481	5.972
16.0	6.14	6.25	0.505	0.795	5.555	6.079
21.2	6.71	6.69	0.541	0.518	6.225	7.075
26.0	7.04	7.14	0.497	0.554	6.402	7.345
30.6	7.24	7.27	0.536	0.577	6.868	8.067
40.0	8.10	7.58	0.747	0.535	7.228	8.635

^a Referred to [13].

^b Referred to [16].

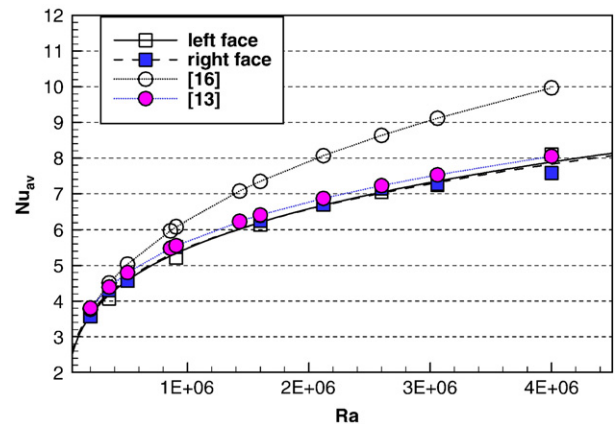


Fig. 12. Comparison between numerical and experimental results.

3.3. Flow field

The flow patterns illustrated in Figs. 9 and 10 are given by flood-type vorticity contours labeled from -2 to 2 with a vorticity increment of 0.4 . For $Ra=1.6 \times 10^6$, the flood-type contours of vortices in the z -direction in the midplane of $z=0$ is shown in Fig. 9. In Fig. 9(a), it is found that the flow pattern at the instant $t=20$ has an excellent symmetry with respect to the origin ($x=y=0$), indicating that the heat transfer rate from the heated vertical wall should be identical to the cooling vertical wall. At this instant, the cellular structures merely occur in the region close to the top and bottom walls.

However, as the heat transfer on vertical direction continues, this excellent symmetry of flow structure has to be broken up. The wall jet margin becomes folding owing to the occurrence of the cellular structures in the cavity central region, as seen in Fig. 9(b)–(c). The comparison between Fig. 9(b)–(c) indicates that the flow pattern should be time dependent, and the instantaneously occurred turbulent flow pattern has no absolutely symmetrical property. This concluding remark can also be confirmed by observing the vortical fields of ω_y at the instants of $t=80$ and 160 shown in Fig. 10(a)–(b).

3.4. Heat transfer

The numerical results were summarized in Table 1, in which the Ra dependence of the face-averaged Nusselt numbers and their rms values were presented. The list of rms of Nusselt numbers in Table 1 shows that the standard deviation of the face-time-averaged Nusselt number varies in the range from 6 to 12.7% for the Rayleigh number varying from 2×10^5 to 4×10^6 .

Because the temperature profiles in the two wall jets are distinguished due to the evolution of asymmetrical turbulent flow structures such as in Figs. 9 and 10, it can be seen that there is a small difference between the averaged Nusselt numbers on the left and right faces, while the difference of their rms is significant when $Ra=1.6 \times 10^6$ and 4×10^6 , but small rms are found for other cases. When $Ra=1.6 \times 10^6$ and 4×10^6 , the evolutions of the face-averaged Nusselt numbers have been given in Fig. 11. It can be seen that the Nusselt numbers on the left and right vertical walls have different temporal oscillating histories.

As seen in Fig. 12, the current numerical results agree with the empirical expression of Mihiev [13] ($Nu_{\text{exp}}=0.18Ra^{0.25}$) quite well, implying that the present coarse grid DNS is also consistent with the early experimental fitting of Emery and Chu [14].

4. Conclusions

The 3D turbulent natural convection in a differentially heated air-filled tall cavity with a height–depth–width ratio of $16:8:1$ is numerically studied in this paper. It was found that the face-time-averaged Nusselt number relates to the Rayleigh number in terms of a power law with an index of 0.25 and the velocity correlation coefficient in the central region of the vertical

centerline of spanwise midplane is spatially oscillating around a value of 0.4 . This wavy distribution is caused by the interaction between the vortical clusters whose evolution is sensitive to the Rayleigh number.

The numerical results agree well with the experimental data of early Russian works. There is also a quantitative consistency of the time-averaged velocity and temperature profiles in the vertical and the horizontal centerlines of the spanwise midplane with recent measurement based on the technique of Laser Doppler anemometry and hotwire probe. The numerical solutions also show that the flow fields in the tall cavity at high Rayleigh numbers must lose their symmetries and become fully turbulent.

Acknowledgements

The work was supported by the FCLU Dean research fund and CERG grand of PolyU, the State Key Laboratory of Fire Science with Grant No. HZ2005-KF01, and NSFC(10572135).

References

- [1] B.I. Shraiman, D.E. Siggia, Scalar turbulence, *Nature* 405 (2000) 639–646.
- [2] K. Hanjalic, One-point closure model for buoyancy-driven turbulent flows, *Annual Review of Fluid Mechanics* 34 (2002) 321–347.
- [3] R. Benzi, Getting a grip on turbulence, *Science* 301 (2003) 605–606.
- [4] H.X. Yang, Z.J. Zhu, Numerical study of turbulent Rayleigh–Benard convection, *International Communication of Heat Mass Transfer* 33 (2006) 184–190.
- [5] F. Wu, Non-standard picture of turbulence, 2004 (Preprint at <<http://arXiv:physics/0308012>>).
- [6] F. Wu, Some key concepts in nonstandard analysis theory of turbulence, *Chinese Physics Letters* 22 (2005) 2604–2607.
- [7] J. Salat, S.H. Xin, P. Joubert, F. Penot, P. Le Quere, Experimental and numerical investigation of turbulent natural convection in a large air-filled cavity, *International Journal of Heat and Fluid Flow* 25 (2004) 824–832.
- [8] Z.J. Zhu, H.X. Yang, Numerical investigation of transient laminar natural convection of air in a tall cavity, *Heat and Mass Transfer* 39 (2003) 579–587.
- [9] P.L. Betts, I.H. Bokhari, Experiments on turbulent natural convection in an enclosed tall cavity, *International Journal of Heat and Fluid Flow* 21 (2000) 675–683.
- [10] J.L. Wright, H. Jin, K.G.T. Hollands, D. Naylor, Flow visualization of natural convection in a tall, air-filled vertical cavity, *International Journal of Heat and Mass Transfer* 49 (2006) 889–904.
- [11] D.L. Brown, R. Cortez, M.L. Minion, Accurate projection methods for the incompressible Navier–Stokes equations, *Journal Computational Physics* 168 (2001) 464–499.
- [12] X.H. Yang, Z.J. Zhu, Exploring super-critical properties of secondary flows of natural convection in inclined channels, *International Journal of Heat and Mass Transfer* 47 (2004) 1217–1226.
- [13] M. Mihiev, *Fundamentals of Heat Transfer*, National-Thermodynamic Publisher, 1956, pp. 1–392, (In Russian).
- [14] A. Emery, N.C. Chu, Heat transfer across vertical layers, *Journal of Heat Transfer* 87 (1965) 110–116.
- [15] H. Tennekes, J.L. Lumley, *A First Course in Turbulence*, MIT Press, Cambridge, MA, 1972.
- [16] S.M. Elsherbiny, G.D. Raithby, K.G.T. Hollands, Heat transfer by natural convection across vertical and inclined air layers, *Journal of Heat Transfer* 104 (1982) 96–102.